Hilary Term 2023

B1 Project A: Analysis of Free Flight Data

Candidate Number: 1073049

Theory and equations in this report are based on ”Simulation of Free Flight Data” by Di Mare and Doherty [1].

1 Introduction

Free flight data captures the motion and trajectory of an aerodynamic body. Obtaining such information is significant in aerodynamic vehicle development, and therefore it is critical to be able to simulate free flight computationally. In this project, this will be achieved by solving a series of problems, introducing additional complexities at each stage.

The general approach is to progress step-by-step, starting with inviscid, thick and steady conditions using the panel method. By dividing the body into panels of finite elements, the body's overall motion is obtained through analysing the forces at, and the interactions between, each panel. Then, unsteadiness will be implemented, introducing complexities like vortex shedding. Finally, shifting to the boundary layer method, viscosity will enter and the interactions between the boundary layer and potential flow will be studied.

This report will start with background on the concept of free flight. Then, the panel and boundary layer methods will be introduced, covering how both methods model a lifting surface. The progression of models will subsequently be validated against existing data from "Theory of Wing Sections" by Abbott & Von Doenhoff [2] and "Low-Speed Aerodynamics" by Katz & Plotkin [3], after which the final model will be applied to the real world by generating flight trajectory data and matching to a reference data for optimised aerodynamic parameters. The report will conclude with discussions on the main findings and areas for improvement.

2 Free Flight

Free flight tests capture a range of information with regards to the object's motion throughout a flight. More specifically, free flight data contains information of a body's centre of mass (hereinafter referred to as "CoM") during motion under gravity and the resultant aerodynamic forces.

To obtain such information, certain quantities are set as inputs: aerofoil geometry (NACA profile and number of subdivisions for panels), free stream velocity, time step, time range, physical aerofoil properties (mass, CoM position, moment of inertia about CoM, initial CoM velocity and initial angular position & velocity), atmospheric conditions (pressure at infinity and density & viscosity of air) and aerodynamic constants (H shape factor, κ and C). The aerodynamic constants govern the behaviour of the boundary layer which will be explained later in the report. For now, note that simplifying assumptions are made that the H shape factor, a function of the momentum and displacement thicknesses, remains constant.

Upon input of such quantities, the desired outputs, which can be separated into three groups, are generated at every time step within a specified time range. First, the linear quantities: the body's position in space and its linear velocity. Second, the angular quantities: the angular position and angular velocity about the body's CoM. Third, the aerodynamic forces acting on the body. Aerodynamic coefficients, such as lift and drag, can also be obtained from the data. These dimensionless coefficients characterise the aerodynamic properties of a body, quantifying lift and drag performances in a consistent manner across varying objects.

3 Panel and Boundary Layer Method

The panel method simulates aerodynamic forces on a body, in the potential flow region, through numerical approximation. By taking an object and dividing its surface into n number of discrete elements, it is possible to obtain the fluid velocity at each panel, from which the pressure distribution can also be determined. This is done by placing a flow element, in this case a uniform source distribution of strength σ, on each panel, and evaluating, at the midpoint of every panel, the contributions from the source distributions at every other panel. Boundary conditions must also be set—by imposing the impermeability condition, requiring that the normal velocity be zero across the entire surface, n equations are realised, and they are subsequently solved to determine the source strengths at each panel. In general, this method is valid in both 2D and 3D, as well as for other types of flow elements beyond a uniform source distribution.

Furthermore, the potential flow must be uniquely determined to obtain a physical solution. Aerofoils are a good example of this, where, with a non-zero angle of incidence, it is clear that there is only one solution that results in finite velocity at the trailing edge. To achieve this, the Kutta condition is applied, generating one further equation that provides the circulation around the body.

The velocity field, due to a uniform source distribution of strength σ_j at each panel, is evaluated using Equation 1. The panel is positioned on the interval $[x_0, x_1]$ on the x axis, and the velocity is evaluated at the general point (x, y). The velocity field due to a uniform vorticity distribution is identical, except that the u and v components are swapped and one of them made negative.

$$\boldsymbol{w} = \begin{bmatrix} u \\ v \end{bmatrix} = \frac{\sigma}{2\pi} \begin{bmatrix} \log \sqrt{\frac{(x-x_0)^2+y^2}{(x-x_1)^2+y^2}} \\ \tan^{-1}\left(\frac{y}{x-x_1}\right) - \tan^{-1}\left(\frac{y}{x-x_0}\right) \end{bmatrix}, \tag{1}$$

Equation 1 can be extended to a panel of general orientation, where the new velocity field is given by $w_{gen} = u\boldsymbol{t} + v\boldsymbol{n}$. u and v are the velocity components from Equation 1.

3.1 Inviscid, Thick and Steady Conditions

In practice, the Hess-Smith panel method is used. First, the panels are generated for an aerofoil of specified NACA profile. Then, the impermeability and Kutta conditions are applied to obtain the equations needed to solve the potential flow problem in determining the source strengths at each panel. This is done by using the aerodynamic influence matrix a (*Eqn. 2*) and the residuals (*Eqn. 3*).

$$a_{ij} = \boldsymbol{n}_i \cdot \boldsymbol{v}_j(x_i, y_i), \tag{2}$$

$$\boldsymbol{v} \cdot \boldsymbol{n}_i = \boldsymbol{n}_i \cdot (\boldsymbol{v}_\infty + \sum_j \Gamma_j \boldsymbol{v}_j(x_i, y_i)) = 0, \tag{3}$$

Note that the Kutta condition is satisfied by applying a uniform vorticity distribution to every panel, where the vorticity is constant across the surface of the object. Once the source strengths are computed, the tangential velocities above each panel are calculated using Equation 1 as combined contributions of the source and vorticity distributions from all panels. Finally, the tangential velocities can be used to obtain the pressure distribution around the aerofoil, allowing for the calculation of pressure, lift and moment coefficients.

3.2 Inviscid, Thick and Unsteady Conditions

Vortex shedding in the wake is introduced when steady flow turns unsteady. To assimilate shed vorticity, one must use Kelvin's theorem of circulation conservation. When unsteadiness causes variations in the circulation around a body, the time derivative of the body and its wake's flow system circulation must remain zero. This means that vortex shedding in a body's wake can be represented by panels, starting from the trailing edge, with its vorticity constant over time. As a result, at each time increment, only the strength of the first wake panel (the latest vortex formed at the trailing edge) is required as new information.

In practice, the addition of unsteadiness can be realised as a modification to Section 3.1. In addition to the existing procedures, one must generate panels to represent the vortex shedding in the wake, updating the vortex panel and vortex core positions, as well as creating a new panel, at every time increment. It is also necessary to calculate the vortex strengths Γ_p at each panel in the wake by solving the unsteady problem. Once the vortex shedding is set up, it is possible to determine the aerodynamic effects of the vortices on the body itself using Equation 4 to calculate their velocity contributions. Equation 4 obtains the velocity field induced at a location (x, y) by a vortex at wake panel p. Now, tangential velocities can be determined at

each panel and the subsequent calculation of aerodynamic coefficients is identical to Section 3.1.

$$\boldsymbol{w} = \begin{bmatrix} u \\ v \end{bmatrix} = \Gamma_p \frac{1}{(x-x_p)^2+(y-y_p)^2} \begin{bmatrix} -(y-y_p) \\ x-x_p \end{bmatrix}, \tag{4}$$

3.3 Viscid, Thick and Unsteady Conditions

In reality, the aerodynamic interactions of a body involve more than just the potential flow region. The boundary layer method also considers the thin layer of fluid near the surface of the body where viscosity is in effect.

The potential flow and boundary layer regions are intertwined with each other, where the boundary layer growth affects the potential flow and vice versa. Specifically, this occurs at the edge of the boundary layer, and the interaction can be expressed by adapting the impermeability condition in the inviscid case—at each panel, rather than setting the normal velocity u_n to zero, it is as shown in Equation 5. δ^* is the displacement thickness and u_e is the velocity at the edge of the boundary layer, obtained from the inviscid solution.

$$u_n = \frac{\partial \delta^*}{\partial t} + \frac{\partial}{\partial x} u_e \delta^*, \tag{5}$$

$$C_f = \frac{2}{(\frac{1}{\kappa} \log Re_\theta + C)^2}, \tag{6}$$

This method builds on the panel method in Sections 3.1 and 3.2, allowing for the calculation of the friction coefficient C_f. In this project, C_f is assumed to be a function of the momentum thickness θ as shown in Equation 6, where κ and C are constants to be determined by optimising the fit between generated data and supplied data. This optimisation process will be explained in detail later in Section 5.

4 Validation

4.1 Aerofoil Geometry

The foundation of this project lies in producing the panel geometry of NACA aerofoils. In total, four geometry functions were used. First, nacaxxxx.m, which generates aerofoil coordinates given a NACA code and the subdivision number along the camber line. Second, naca00xxc.m, which generates camber line coordinates given the height & position of maximum camber and the “horizontal” locations at which the coordinates are needed. Third, naca00xxt.m, which calculates the thickness given the thickness value and the “horizontal” locations at which the coordinates are needed. Last, attitude.m, which outputs tilted

coordinates of an input aerofoil geometry given the CoM position and incidence angle. These codes were tested on NACA 4415, 0015 and 2412. Figures 1, 2 and 3 validate the correct operation of the geometry functions against data from Appendix 3, "Theory of Wing Sections" [2]. Whilst only plots of NACA 4415 are shown in this report, the validation results were accurate and consistent for the two other aerofoils as well.

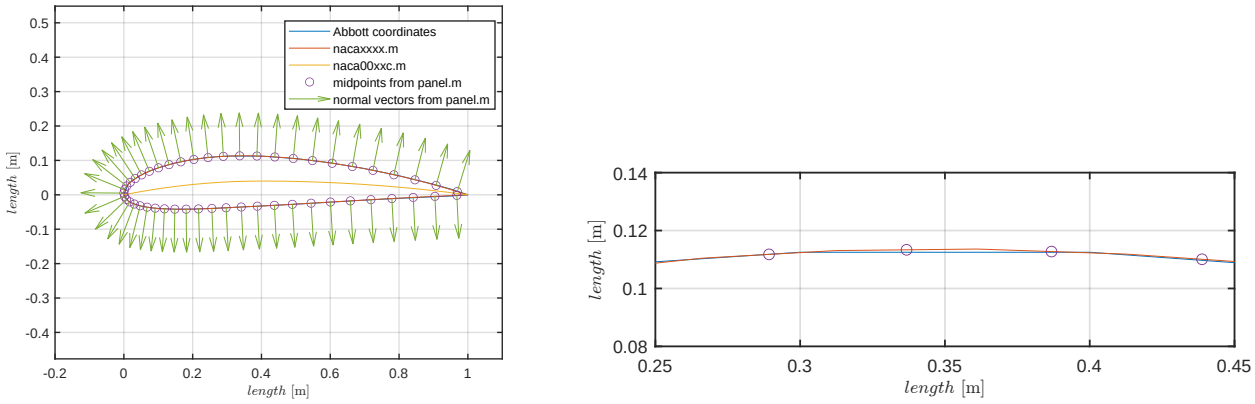

(a) Aerofoil geometry

(b) Zoomed figure

Figure 1: Validation of aerofoil functions on NACA 4415, along with a zoomed-in plot for clarity.

4.2 Uniform Source/Vortex Distribution

Following the geometry functions, code must be written to place a uniform source and vortex distribution on the panels. The code, which takes the two endpoints of a panel and the location where the induced velocity is required, first obtains the panel's tangent and normal vectors, $\boldsymbol{t}$ and $\boldsymbol{n}$. Then, the panel is "rotated" to put into a "horizontal" reference frame where Equation 1 can be applied. Finally, the velocity components u and v, calculated from Equation 1, is converted back to the original reference frame. This function is validated using quiver plots (*Fig. 4*) for a panel with vertices $(0,0)$ and $(1,1)$.

4.3 Inviscid, Thick and Steady Conditions

With the geometry and source functions in place, it is possible to simulate the inviscid, thick and steady problem. To do this, a nested for-loop was written to loop through each panel, and at each panel further loop through all panels to sum the velocity contributions from their sources and vortices. Essentially, Equation 1 was applied repeatedly with the different strength values of the respective panels. Once the tangential velocities were obtained for all panels, their pressure coefficients C_p were calculated using Equation 7, where v_∞ is the free stream velocity. Then, using the C_p values generated, the lift coefficient C_l and moment

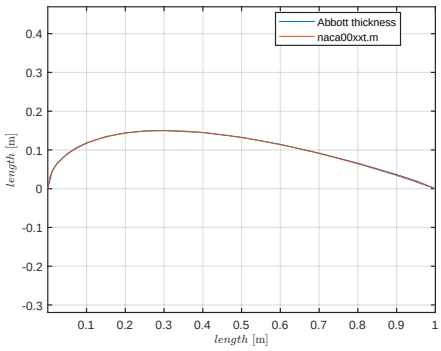

Figure 2: Validation of thickness function on NACA 4415.

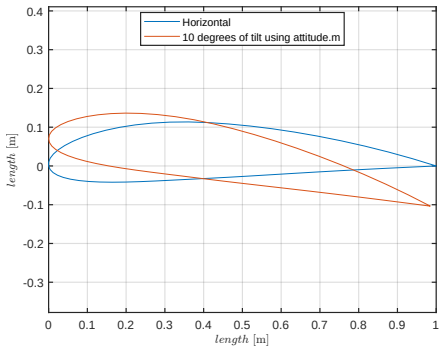

Figure 3: Validation of attitude function on NACA 4415.

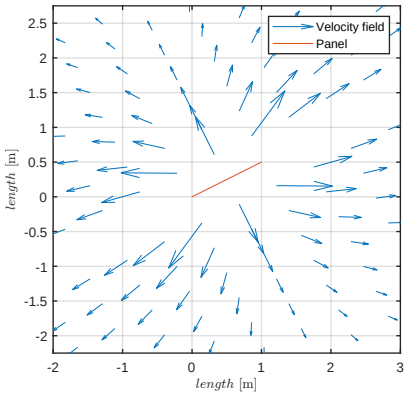

(a) Uniform source distribution

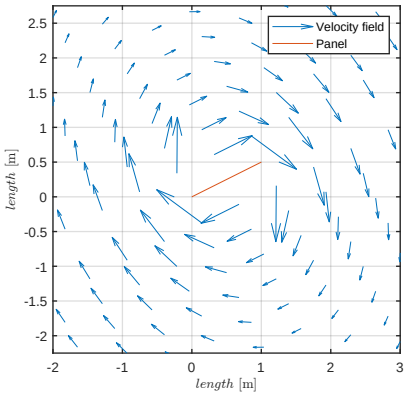

(b) Uniform vorticity distribution

Figure 4: Validation of uniform distribution function on a panel (unit source strength).

coefficient C_m were subsequently computed with Equations 8 and 9 respectively.

$$C_{p_i} = 1 - \frac{v_i^2}{v_\infty^2}, \tag{7}$$

$$C_l = \sum_{i=1}^{n} C_{p_i} s_i \hat{\boldsymbol{n}}_i \cdot \begin{bmatrix} 0 \\ 1 \end{bmatrix}, \tag{8}$$

$$C_m = \sum_{i=1}^{n} C_{p_i} s_i \hat{\boldsymbol{n}}_i \cdot \begin{bmatrix} 0 \\ 1 \end{bmatrix} (x_{CoM} - x_i) \cos\alpha, \tag{9}$$

To validate this problem, the C_p values for NACA 0015 were plotted in Figure 5 against data from Appendix 1, Abbott & Von Doenhoff [2]. The two plots are almost identical, validating our method for pressure coefficients. Next, C_l and C_m plots (*Fig. 6*) for NACA 0012 are compared side-by-side with a figure from Appendix 4, Abbott & Von Doenhoff [2]. It is noticeable that Figure 6a exhibits stall effects, unlike Figure 6b. This is expected since the generated data was simulated under inviscid conditions, unlike viscous conditions for the data from Abbott & Von Doenhoff [2]. For this reason, it is only possible to validate an angle of attack

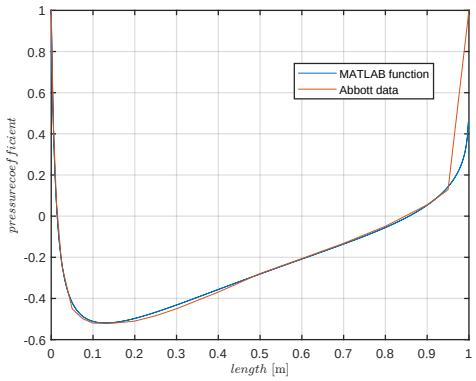

Figure 5: Validation of NACA 0015 pressure coefficient data under inviscid, thick and steady conditions.

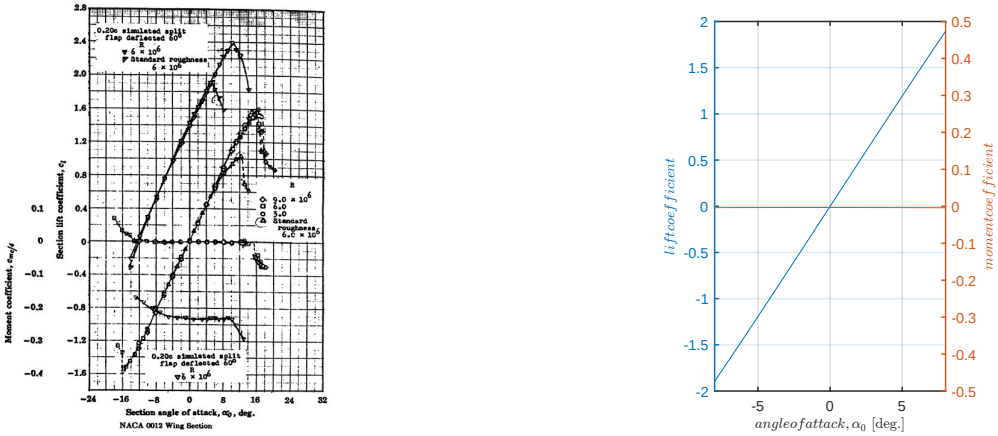

(a) Data from Abbott & Von Doenhoff [2]

(b) Generated data

Figure 6: Validation of NACA 0012 lift and moment coefficient data under inviscid, thick and steady conditions.

of range $\alpha_0 = -8$ to $+8$. Otherwise, the two data are consistent with each other. Subtle differences in the magnitude of the lift coefficients can be attributed to miscellaneous differences in simulating conditions.

4.4 Inviscid, Thick and Unsteady Conditions

This problem is similar to Section 4.3, with the addition of time integration to evaluate the effects of vortex shedding in the wake. In practice, this was executed by adding an additional loop inside the first loop to iterate through all the "old" wake panels created at each time step and evaluating their velocity contributions at each panel using Equation 4. To validate this problem, circulation $\Gamma(t)$ over $\Gamma(t = \infty)$, was plotted over time (*Fig. 7b, 7c*) and compared to Figure 13.8 from Katz & Plotkin [3]. Consistency can be seen amongst the plots in Figure 7. Whilst Figure 7a portrays the sudden acceleration of a flat plate instead of an aerofoil, comparisons with aerofoils or other streamlined objects are valid since the starting vortex at $t = 0$ has the most significant effect on lift—as the starting vortex moves away, it tends towards steady state. This can be verified by comparing Figures 7b and 7c, where doubling the aerofoil thickness outputs similar results.

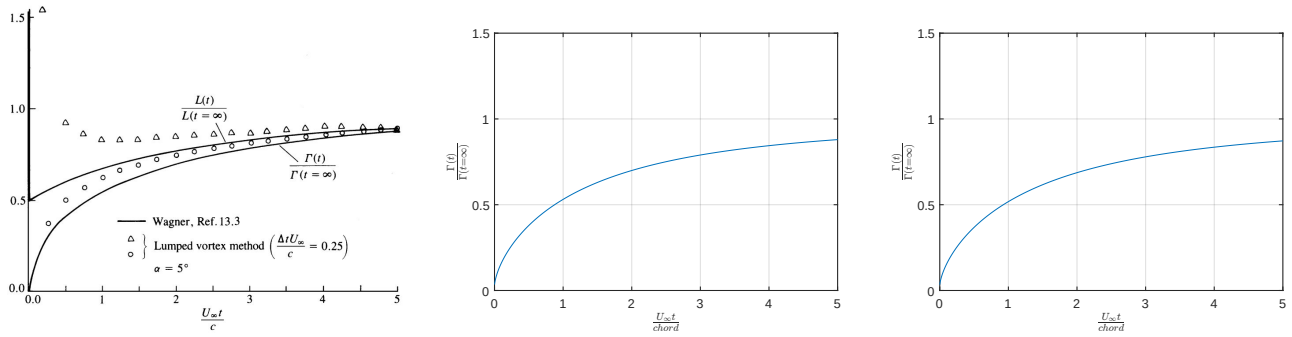

(a) Data from Katz & Plotkin [3] **(b)** Generated data for NACA 0006 **(c)** Generated data for NACA 0012

Figure 7: Validation of circulation data under inviscid, thick and unsteady conditions.

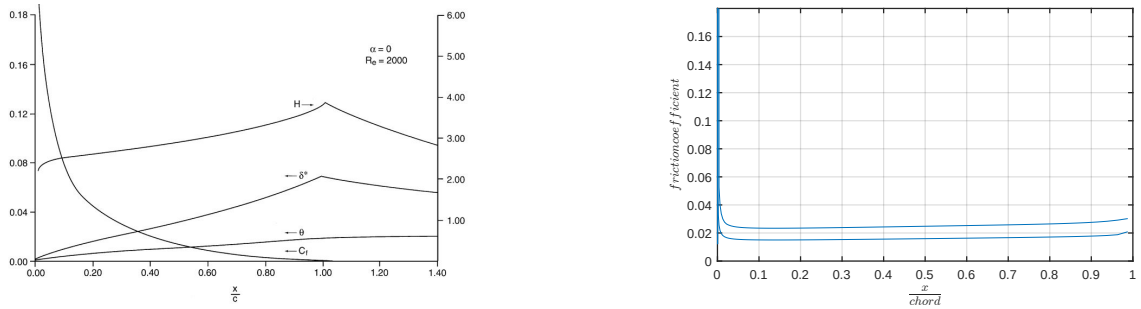

(a) Data from Katz & Plotkin [3] **(b)** Generated data

Figure 8: Validation of NACA 0012 friction coefficient data under viscid, thick and unsteady conditions.

Note that, for this reason, the circulation at $t = \infty$ was simply retrieved from the problem in Section 4.3.

4.5 Boundary Layer Behaviour

To validate the boundary layer method, the friction coefficient C_f was plotted (*Fig. 8b*) and compared with Figure 14.13 from Katz & Plotkin [3]. In practice, the friction coefficients were obtained by commenting out the section of code that advances the force & angular momentum balances in time, then retrieving the values of boundary layer edge velocity u_e and displacement thickness δ^* at the last time step. Then, C_f values were computed for each panel using Equation 6, where Re_θ is obtained by Equation 10. Whilst the two plots in Figure 8 do not match perfectly, the key features are consistent: the singularity at $x = 0$, the leading edge, and the subsequent curve that tends towards zero. Considering that the data from Katz & Plotkin [3] was simulated under laminar conditions rather than the turbulent conditions for Equation 6, it can be concluded that the two plots are sufficiently consistent and valid.

$$Re_{\theta_i} = \frac{\rho_\infty u_{e_i} \delta^*{}_i}{\mu_\infty}. \tag{10}$$

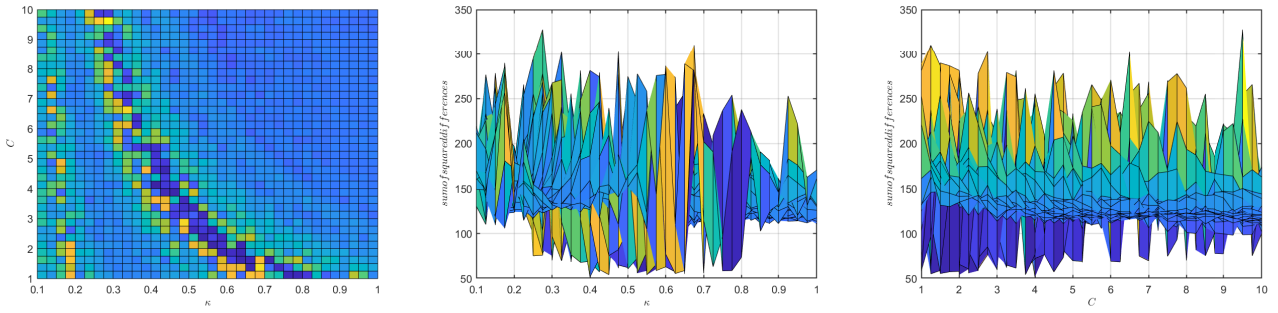

(a) 2D view **(b)** Squared difference sum across κ **(c)** Squared difference sum across C

Figure 9: First iteration of flight trajectory matching process.

5 Application

The flight trajectory data is output in the form of a matrix with 9 columns and as many rows of time increments as set. The 9 columns contain information on the x and y components of the aerodynamic force, CoM velocity & position, as well as the moment and angular velocity & position about the CoM.

To test real-world applications of the free flight model, trajectory data was generated and compared with reference data. The generated data was fit to the reference data to obtain values for κ and C in Equation 6. The matching procedure was executed by an optimisation code that implemented a nested for-loop to test every combination of κ and C within a given range, generating trajectory data with said combination and computing the sum of the squares of the differences between the generated and reference trajectories. The squared difference sum were stored in a matrix to output a surface plot (*Fig. 9, 10*) for visualisation of the κ and C values that resulted in the closest match to the reference data.

To minimise computing duration, the optimisation process was divided into iterations with decreasing range and increasing resolution. The first iteration (*Fig. 9*) was conducted from $\kappa = 0.10$ to 1.00 in 0.025 intervals and $C = 1.0$ to 10.0 in 0.25 intervals. Upon identifying the minimum at this first resolution, a second iteration was set up to study a narrower range of values around the identified minimum at a higher resolution to discover further "hidden" minima. This approach was applied consistently through to the sixth and final iteration (*Fig. 10*). Table 1 shows the set of values analysed at each iteration.

#	κ_1	κ_2	κ_{int}	C_1	C_2	C_{int}
1	0.100	1.000	0.025	1.00	10.00	0.25
2	0.350	0.800	0.010	1.00	5.00	0.10
3	0.400	0.625	0.005	1.25	3.25	0.05
4	0.430	0.480	0.0025	2.70	3.20	0.025
5	0.445	0.455	0.0005	2.85	2.95	0.005
6	0.449	0.451	0.0001	2.89	2.91	0.001

Table 1: Values of κ and C, as well as their increments, used in the trajectory matching process.

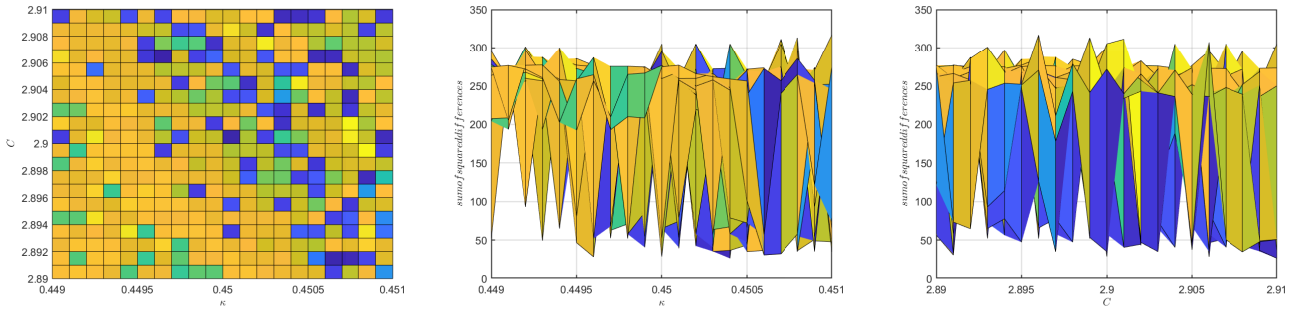

(a) 2D view **(b)** Squared difference sum across κ **(c)** Squared difference sum across C

Figure 10: Final iteration of flight trajectory matching process.

6 Summary and Conclusions

The main findings are the optimised aerodynamic parameters identified at the minimum in the final iteration (*Fig. 10*) in Section 5. The values were $\kappa_{opt} = 0.4504$ and $C_{opt} = 2.910$, giving a squared difference sum of 26.2838 when compared to the reference trajectory.

An area for improvement for the trajectory matching procedure is the resolution. In essence, the goal is to obtain deeper and better defined ”valleys” for greater contrast. Despite six iterations and over a dozen hours of run time, the optimised values still return a trajectory with significant error. Initially, to increase resolution, the matching process was shortened to one tenth of the total time range. Whilst this returned results with significantly higher resolution, they were invalid due to the nature of free flight trajectory. Projectile trajectories are largely similar at early times—it is only at later times that aerodynamic parameters begin to exhibit significant effects. In addition, whilst the ”valleys” were better defined, they were significantly more shallow compared to analyses of the full time range. Therefore, it is critical to study the full time range of a flight.

One potential idea to improve resolution whilst analysing the full time range is to ”skip” time increments rather than narrow down to early times. This will capture the entire trajectory whilst decreasing computing time and power, allowing for higher resolution. A more rigorous and brute-force method would be to use a more powerful computer to complete the procedure in Section 5 with higher resolution in shorter time. By implementing such ideas, it may be possible to further identify any minima that were ”hidden” in Section 5, returning better optimised aerodynamic parameters with trajectories closer to the reference trajectory.

References

[1] Luca Di Mare and Luke Doherty. B1 Project: Simulation of Free Flight Data, 2022.

[2] I. H. Abbott and A. E. Doenhoff. *Theory of Wing Sections: Including a Summary of Airfoil Data*. June 1959.

[3] Joseph Katz and Allen Plotkin. *Low-Speed Aerodynamics*. Cambridge Aerospace Series. Cambridge University Press, Cambridge, 2 edition, 2001.